NeuroImage: Clinical 47 (2025) 103827

Contents lists available at ScienceDirect

NeuroImage: Clinical

journal homepage: www.elsevier.com/locate/ynicl

Fully automated pipeline for the fiber tractography of the anterior optic pathway in patients with sellar and parasellar tumors and analysis of the microstructural alterations

Laura Ludovica Gramegna [a,b,*,1], Matteo Zoli [a,c,1], Giovanni Sighinolfi [b], Alessandro Carrozzi [d], Gianfranco Vornetti [a,b], Elena Cantoni [b], Federica Guaraldi [c], Sofia Asioli [a,c], Caterina Tonon [a,b,*], David Neil Manners [b,e], Diego Mazzatenta [a,c,1], Raffaele Lodi [a,b,1]

[a] Department of Biomedical and Neuromotor Sciences (DIBINEM), University of Bologna, Bologna, Italy
[b] IRCCS Istituto delle Scienze Neurologiche di Bologna, Functional and Molecular Neuroimaging Unit, Bologna, Italy
[c] IRCCS Istituto delle Scienze Neurologiche di Bologna, Pituitary Unit, Bologna, Italy
[d] Department of Medical and Surgical Sciences (DIMEC), University of Bologna, Bologna, Italy
[e] Department for Life Quality Studies (QUVI), University of Bologna, Bologna, Italy

ARTICLE INFO

Keywords:
Anterior optic pathway
Diffusion fiber tractography
Endoscopic endonasal surgery
Magnetic resonance imaging
Sellar tumors

ABSTRACT

Compared to conventional morphological MR imaging, diffusion tractography may improve the visualization of the anterior optic pathway (AOP), thus enhancing the understanding of its anatomical relationship with surrounding sellar/parasellar tumors (SPTs).

We aimed to develop a diffusion tractography pipeline for automatic and reliable reconstruction of the AOP and to investigate its microstructural alterations in SPT patients.

A multishell diffusion protocol (b-values = 0,300,1000,2000 s/mm^2; 64 maximum gradient directions; 2-mm isotropic voxel) on a 3T scanner, followed by a fully automated pipeline developed in-house to perform the probabilistic tractography, based on multishell-multitissue constrained spherical deconvolution modeling of the signal, was performed. It was first tested retrospectively in 10 healthy controls, then prospectively applied in 25 additional healthy controls and 35 SPTs patients. Microstructural parameters were compared between patients and controls using an along-tract approach.

The study included 70 subjects: 35 healthy controls (18 females, mean age 50.7 ± 14.3 years) and 35 patients with SPTs displacing the optic chiasm (18 females; mean age 53.7 ± 16.4 years). The AOP reconstruction was successfully performed in all normal controls and patients. A correct correspondence with surgical inspection was identified in 84.7 % of patients who underwent surgery. Patients had significantly lower mean diffusivity (MD) values at the level of the chiasm ($p < 0.01$), that correlated with supero-inferior chiasmatic displacement ($R = -0.49$, $p = 0.01$).

A novel, fully automated diffusion tractography pipeline for the AOP was developed and validated in patients with sellar/parasellar tumors. Reduced MD values at the chiasm level may indicate compression or gliosis in case of displacement.

1. Introduction

Anatomical visualization of the anterior optic pathway (AOP), including optic nerves, chiasm, and optic tracts, is a topic of great interest for neurosurgeons dealing with sellar and parasellar tumors (SPTs), as lesions extending to the suprasellar region may compress AOP fibers (Carrozzi et al., 2023). The definition of the anatomical relationship between the chiasm and the tumor is of great importance in the selection and planning of the surgical approach (Zoli et al., 2022), and intra-operatively for minimizing the risk of damage to the visual system.

From a neuroradiological perspective, the visualization of cranial nerves (CNs) has historically relied on magnetic resonance imaging

* Corresponding authors at: Department of Biomedical and Neuromotor Sciences, University of Bologna, Via Altura 3, Bologna 40139, Italy.
E-mail addresses: lauraludovica.gramegna@unibo.it (L.L. Gramegna), caterina.tonon@unibo.it (C. Tonon).
[1] These authors equally contributed to this manuscript.

https://doi.org/10.1016/j.nicl.2025.103827
Received 12 February 2025; Received in revised form 10 June 2025; Accepted 15 June 2025
Available online 16 June 2025

(MRI) steady-state acquisition sequences (Mikami et al., 2005). These sequences generate contrast based on the distinction between the cerebrospinal fluid (CSF) and the cranial nerve tissue (Mikami et al., 2005). Therefore, they often lack adequate contrast between the nerve and the tumor tissue and do not provide sufficient information regarding the continuity and integrity of the nerve tracts (Castellaro et al., 2020).

Diffusion fiber tractography is an advanced MRI technique based on multiple oriented magnetic field gradients sensitive to the random microscopic motion of water molecules (i.e., diffusion), capable of measuring the differential dephasing of spins of protons in water molecules due to the presence of structures that act as barriers to diffusion (Basser et al., 2000). The application of tractography in the central nervous system relies on the assumption that, in the human brain, the main barriers responsible for this anisotropic diffusion are the myelinated white matter tracts (Jones, 2010), such as the CNs (Puzniak et al., 2019).

Important ongoing issues that limit the use of CN tractography in clinical practice include the absence of standardized and automated acquisition and analysis methods, as well as a lack of validation regarding the anatomical accuracy of the reconstructions (Carrozzi et al., 2023).

Some previous studies have reported on the feasibility of performing CN tractography of AOP tracts (Carrozzi et al., 2023; Jacquesson et al., 2018a; He et al., 2021). However, the peculiar course of the AOP poses several challenges for diffusion weighted imaging (DWI) data acquisition and tractography reconstruction. First, the various segments of the AOP are surrounded by fat, muscle, bone, and air-filled sinuses, each contributing to MRI signal distortion due to partial volume and magnetic susceptibility artifacts. Additionally, fiber crossings in the optic chiasm can lead to tracking errors if the tractography technique employed cannot handle multiple fiber orientations within a voxel (Jeurissen et al., 2017). Moreover, the presence of a tumor that can significantly alter brain morphology at the skull base further complicates the challenge of achieving high-quality tractography, especially in an automated pipeline design.

For these reasons, tractography reconstruction is still not routinely employed for the study of AOP in clinical practice, and it is unclear whether the diffusion microstructural parameters are associated with clinical variables.

This study aims to develop and validate a fully automated diffusion tractography pipeline to reliably reconstruct the AOP, also applicable to cases of severely altered morphology, favoring the integration of this non-invasive advanced imaging technique into routine clinical practice. Additionally, we aimed to characterize the microstructural alterations along the course of the AOP in SPT patients compared to healthy controls, in order to deepen our knowledge regarding the tumor impact on the tract fibers.

2. Materials and methods

2.1. Study population

A subsample of 10 healthy controls who had undergone multishell DWI and 3D MPRAGE T1-weighted acquisitions were retrospectively selected from the normative database of MRI exams conducted at the Neuroimaging Laboratory of the IRCSS Institute of Neurological Sciences of Bologna for testing the feasibility of the methodological approach.

Subsequently, 25 healthy adults aged 18 or older and 35 patients with SPTs compressing the AOP structures and candidates for surgical resection, evaluated at the Pituitary Unit of the IRCSS Institute of Neurological Sciences of Bologna between May 2021 and December 2022 were included. Exclusion criteria were previous radiotherapy and contraindications to the MRI scan.

Written informed consent was obtained from all participants before inclusion in the study. The study was conducted according to the Declaration of Helsinki guidelines and approved by the local Ethics Committee (Codice CE 815–2020-SPER-AUSLBO).

2.2. Patient management

All patients underwent a pre- and post-operative standardized assessment at the Pituitary Unit of IRCCS Istituto delle Scienze Neurologiche di Bologna, the regional (Emilia-Romagna, Italy) tertiary referral center for pituitary tumors. Pre-operative evaluations included a neurological examination and an ophthalmological examination, consisting of a computerized visual field assessment; and the evaluation of basal pituitary function (i.e., serum ACTH, cortisol, prolactin, GH, IGF-1, fT4, TSH, sodium, potassium, plasma and urine osmolarity, LH, FSH; testosterone in males or estradiol in females).

Surgery was performed through endoscopic endonasal approach in all cases; for purely suprasellar lesions, an extended transplanum/transtuberculum approach was chosen (Zoli et al., 2022; Barazi et al., 2012). Pathological examinations were performed by an expert neuropathologist, according to the pre-operative clinical suspicion, following the 5th Edition of the WHO Classification of Endocrine and Neuroendocrine Tumors and of Tumors of the Central Nervous System (Gaillard 2025).

Post-operative evaluation included a brain MRI with specialized sequences for the sellar region and paramagnetic contrast injection, conducted at 3 and 12 months to assess the extent of tumor resection. Resection was classified as ‘radical’ if no visible remnants were detected; otherwise, it was considered ‘incomplete.’ Neurological, ophthalmological, and endocrinological outcomes were assessed using the same evaluations performed at enrollment.

2.3. Brain MRI acquisition

Images were acquired using a 3 T MRI scanner (Magnetom Skyra, Siemens, Erlangen, Germany) with VE11C-SP01 software (maximum gradient amplitude 45 mT/m; maximum “slew rate” 200 T/m/s) and a 64-channel phased head coil. A standardized scan protocol was performed including, as an anatomical reference, a 1 mm isotropic 3D magnetization-prepared rapid gradient-echo (3D MPRAGE) T1-weighted sequence (TE = 2.98 ms, TR = 2300 ms, TA = 5:21 min) followed by 0.5 mm isotropic 3D constrained interference steady state (CISS) (TE = 3.81 ms, TR = 8.36 ms, TA = 09:07 min). DWI multishell acquisition [12] was employed with a single-shot spin-echo EPI sequence, repeated with anterior-posterior (A-P) and posterior-anterior (P-A) phase-encoding directions (TE = 98 ms, TR = 4300 ms, 2 mm isotropic voxel, TA = 12:45 min), acquiring a total of 164 volumes with the following scheme: 8 directions at b = 0 s/mm^2 (A-P and P-A), 12 at b = 300 s/mm^2 (A-P and P-A), 30 at b = 1000 s/mm^2 (A-P and P-A), 64 at b = 2000 s/mm^2 (A-P). Coronal and sagittal turbo spin echo (TSE) sequences T1- (TE = 8.1 ms; TR = 650 ms; 2 mm thick slices, TA = 03:21 and 04:51 min respectively) and coronal T2-weighted (TE = 99 ms; TR = 4000 ms, TA = 02:14 min) were acquired centered on the sellar region. Finally, after paramagnetic contrast agent administration (Gadoteridol 0.2 cc/kg) coronal T1-weighted coronal TSE, sagittal T1-weighted coronal TSE, and 3D MPRAGE T1-weighted were repeated. Written informed consent was obtained from all participants before MRI examination.

2.4. Imaging preprocessing

MRI data of each participant were preprocessed using an automated pipeline developed in-house based on freely available software packages as part of FSL (Jenkinson et al., 2012), version 6; the NIH AFNI suite (Cox, 1996), version 20.3.02; and MRtrix3 (Tournier et al., 2012), version 3.0.2, as previously reported (Veraart et al., 2016; Dhollander et al., 2019; Manners et al., 2022) (see Supplementary Material Part 1 for details).

2.5. Anterior optic pathway (AOP) tractography

All the regions of interest (ROIs) used for the streamline selection of the AOP were manually defined on the MNI152 standard brain. Seed and inclusion ROIs for streamline generation and selection were drawn in the posterior limit of the orbits, the optic chiasm and the lateral geniculate nucleus (LGN). A mask, broadly encompassing the entire AOP, from the optic bulb to the LGN ROI, was also defined to ensure the truncation of streamlines extending beyond the main tract. Lastly, a single exclusion ROI was defined to remove spurious streamlines, by covering all potential regions where erroneous segments departing in proximity of the AOP could arise. Fig. 1 illustrates the described ROIs on the MNI standard brain. The registration between the MNI and the single-subject DWI was performed using a non-linear warping (see Supplementary Material Part 1), with a nearest neighbor interpolation method for the masks and exclusion ROIs, and with a trilinear interpolation for seed and inclusion ones.

The streamline generation was performed using the iFOD1 (Tournier et al., 2012) method implemented in MRtrix3 'tckgen,' based on the Fiber Orientation Distribution (FOD) estimated via the multishell-multitissue constrained spherical deconvolution model (Jeurissen et al., 2014). Streamlines were seeded from the LGN ROI and then filtered based on specific criteria: crossing inclusion ROIs (chiasm and orbit), crossing voxels with FOD amplitude >0.005 and having a maximum deviation angle of 10° between subsequent voxels. Using this approach, four different types of tracks were separately reconstructed depending on whether they crossed (Left-Right LR, Right-Left RL) or did not cross (Left-Left LL, Right-Right RR) hemispheres through the optic chiasm (decussation). Up to 5×10^6 streamlines could be generated; however, if 1000 streamlines per track were found according to the above-mentioned constraints, the seeding process was halted. The same process was repeated after inverting the seed (LGN) and target (orbit) regions. Finally, all generated tracks were merged into a single one. The resulting tracts were converted into a NIfTI image, where the voxel intensity represented the track density. A 10 % threshold of the maximum value was applied to the resulting image, and it was used to mask the original streamlines so that they would more strictly overlap the anatomical AOP. Lastly, we selected only streamlines whose length was greater than the median length minus 5 standard deviations of the entire tract prior to masking, in order to remove those streamlines that were severely truncated at the last masking step.

The tractography pipeline for the AOP reconstruction was initially defined and tested on the subsample of 10 healthy controls, then extended to the remaining healthy controls and patients. The results were compared with the underlying anatomy by two expert neuroradiologists (LLG and GV) as described in the following subsection.

In addition, an algorithm was developed to automatically adjust the ROI of the chiasm in the cases where this anatomical structure was dislocated by the tumor and therefore the ROI was erroneously located inside the lesion. This method, based on the intensity on T1-weighted images in the chiasmal region, is described in Supplementary Material Part 2.

The entire tractography pipeline was run on a Linux-based server running Ubuntu 20.04.2, equipped with 40 Intel Xeon Gold 6138 CPU cores (2 threads per core) and 251 GiB of RAM. Running the pipeline on a single subject takes a variable time, ranging between 10 and 60 min if parallelized over 10 threads, depending on the number of seeded streamlines needed to achieve the selection constraint. Therefore, the time is typically longer for patients with abnormal anatomy.

Test-retest performances are described in Part 3 of the Supplementary Material. Reproducibility performances on healthy controls are reported in Part 5 of the Supplementary Material.

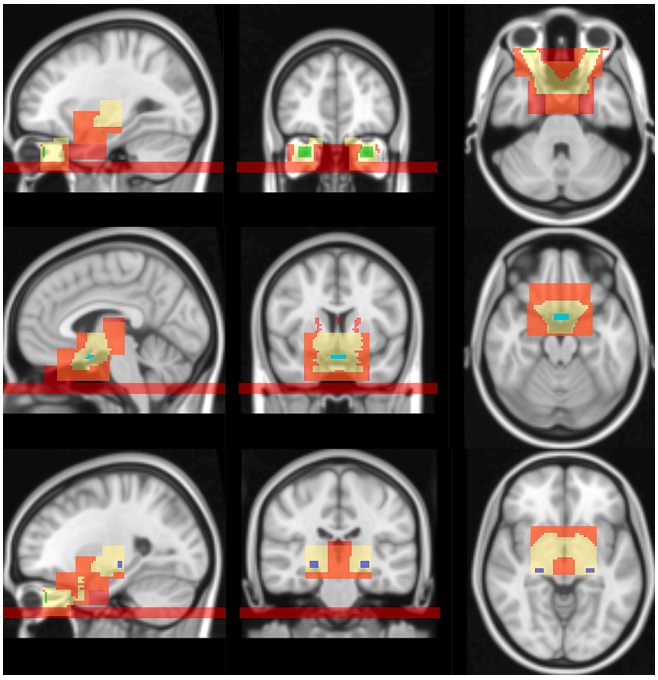

Fig. 1. Regions of interest (ROIs) defined on the MNI standard brain for the streamline selection to reconstruct the anterior optic pathway. The truncation mask including the trajectory of the whole anterior optic pathway from the optic bulb to the lateral geniculate nucleus is depicted in yellow. The exclusion region to remove spurious streamlines originating from the principal tract is depicted in red. Seed/inclusion ROIs in the orbit (green), in the optic chiasm (light blue) and in the lateral geniculate nucleus (blue) are also shown in the sagittal, coronal and axial views. (For interpretation of the references to colour in this figure legend, the reader is referred to the web version of this article.)

2.6. Neuroradiological anatomical comparison

Participants (both healthy subjects and SPT patients) 3D T1-weighted MPRAGE and CISS images were visually inspected by two expert neuroradiologists (LLG and GV), assessing the visibility of the AOP by consensus. For this evaluation, the AOP was divided into five distinct parts: right optic nerve, left optic nerve, optic chiasm, right optic tract, and left optic tract. We employed a three-tier rating system to evaluate the visibility, i.e., discernability, of the five abovementioned structures by the surrounding tissue components (fat, blood vessels, brain parenchyma or solid tissue). This system categorizes visibility into three distinct levels: "Perfectly Visible," "Partially Visible," and "Not Visible." The "Perfectly Visible" rating is assigned when all five structures are visible. The "Partially Visible" rating applies when at least one of the structures is not fully visible, yet at least one remains discernible. Lastly, the "Not Visible" rating is used when none of the five structures can be identified in the image. The time required for the complete visual assessment of the AOP, including its visualization on the CISS, the T1-weighted image and the tractography reconstruction, ranged between 2–5 mins, depending on the complexity of the case.

Fig. 2 shows three illustrative examples corresponding to the three distinct ratings.

In cases where the trajectory of the AOP was identifiable through conventional imaging methods such as 3D MPRAGE T1-weighted imaging, this data was used to confirm the accuracy of the reconstructed tract. In summary, the reconstructed tracts were superimposed onto a 3D MPRAGE T1-weighted image volume and examined visually by an expert neuroradiologist (LLG) to ensure that the course accurately overlaid the features visible on the conventional image.

2.6.1. Chiasmal displacement measurement

The craniocaudal displacement of the optic chiasm was assessed by measuring the bulbopontine height (BP-height; considered a reliable indicator of chiasmal compression), caused by SPTs (Liang et al., 2021).

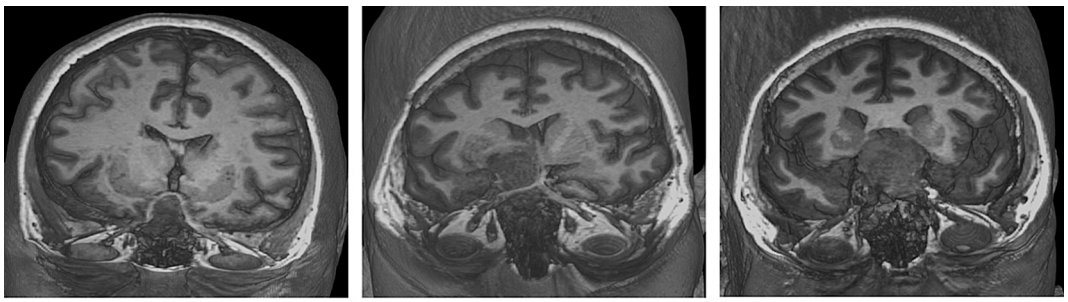

Fig. 2. 3D reconstructions of a 3D MPRAGE T1-weighted image of three different patients with SPTs in which the AOP was visually judged to be "perfectly visible" (left), "partially visible" (center) and "not visible" (right).

The BP-height was measured using 3D T1-weighted MPRAGE images, following the definition reported by Frisen and Jensen (Frisén and Jensen 2008). Briefly, a sagittal line was drawn between the dorsal-most aspect of the olfactory bulbs and the ponto-mesencephalic junction, and the BP-height was measured as the perpendicular distance between the superior aspect of the chiasm and this line at the level of the anterior commissure. BP-height greater than 1 mm was considered to indicate vertical chiasmal displacement.

2.6.2. Imaging transfer to the neuronavigation system

To transfer the images to the neuronavigation system (StealthStation S7 MEDTRONIC, Louisville, CO, US), we registered each anterior optic pathway reconstruction from the DWI space to the 3D MPRAGE T1 using trilinear interpolation. The neuroradiologist visualized the resulting images and selected an intensity threshold if needed. The NIfTI image was then converted to a Digital Imaging and Communications in Medicine (DICOM) format using the open-source Karawun python package (https://github.com/DevelopmentalImagingMCRI/karawun) (Beare et al., 2023) for compatibility with the neuronavigator system.

2.7. Neurosurgical confirmation

In the subgroup of patients with clinical indication to transsphenoidal approach, an extended transplanum-transtuberculum approach was used (Barazi et al., 2012; Carretta et al., 2023). The DWI 3D reconstruction images were transformed into DICOM format and transferred to the neuronavigation system using dedicated software for endoscopic procedures (StealthStation S8, Medtronic, Louisville, CO, USA). For each patient, the fidelity of the five AOP reconstructed portions (right optic tract, left optic tract, optic chiasm, right optic tract, and left optic tract) and the corresponding surgical structures identified intraoperatively were evaluated to determine if the former were fully compliant (yes or no answer).

2.8. Along-tract analysis

To perform the along-tract analysis of the AOP, the tracts were first registered to the MNI using the "tcktransform" tool from the MRtrix3 package. Then, each streamline was resampled to a fixed number of points (45). This number was chosen based on the mean streamline length in the HC group after registration to the MNI (89.7 ± 9.4 mm), divided by the voxel side (2 mm), to ensure at least one sampling point per voxel. These points were divided into three regions along the tract: points 1–20 corresponded to the optic nerve, points 21–28 to the optic chiasm, and points 29–45 to the optic tract.

The FSL "dtifit" tool was used to estimate voxel-wise Fractional Anisotropy (FA) and Mean Diffusivity (MD) based on the diffusion tensor, allowing for the characterization of the microstructural properties of tissue within each voxel.

In addition, a fixel-based analysis was conducted using the "fod2fixel" function of MRtrix3 to retrieve an Apparent Fiber Density (FD) map, which provides a relative measure of the intra-axonal volume occupied by fibers aligned along the corresponding orientation (Raffelt et al., 2012; 2017).

For each subject and microstructural metric, the values were extracted at the sampling point and averaged across streamlines, resulting in an array of 45 along-tract values. This was done separately for streamlines located in the right or left hemisphere, while points within the chiasm were averaged independently of the hemisphere.

2.9. Statistical analysis

Continuous variables were summarized as mean ± standard deviation (SD), while categorical variables were expressed as absolute numbers (n) and percentages (%). Groups were compared using Student's *t*-test or Mann-Whitney *U* test, as appropriate, for continuous variables and Pearson chi-square test or Fisher's exact test, as appropriate, for categorical variables.

Diffusion metrics were compared between patients and controls using an unpaired two-sided *t*-test. Patients presenting with visual symptoms were divided into those who experienced complete or partial resolution of symptoms ('responders') and those who did not ('non-responders) at 6-month follow-up. The two groups of patients were compared using an unpaired *t*-test. The same analysis was also repeated to compare the subgroups of patients with bilateral visual field deficits, right homonymous hemianopia or left homonymous hemianopia with the healthy control group.

The Pearson's correlation between the B-P height and the MD within the chiasm was calculated, based on the hypothesis that displacement would be associated with microstructural changes.

All results were corrected for multiple comparisons using the false discovery rate method (Benjamini and Hochberg 1995). Statistical significance was set at adjusted p-value < 0.05.

3. Results

3.1. Study population

A total of 70 subjects were included in the study. Among them, 35 patients with SPTs compressing or displacing the optic chiasm (18 females; mean age 53.7 ± 16.4 years) and 35 were healthy controls (18 female; mean age 50.7 ± 14.3 years).

The series included twenty (57.1 %) anterior pituitary neuroendocrine tumors (PitNET), nine (25.7 %) tuberculum sellae grade I (WHO CNS 2021) meningiomas, two (5.7 %) grade I (WHO CNS 2021) craniopharyngiomas, one grade I (WHO CNS 2021) (2.9 %) hypothalamic pilocytic astrocytoma, one grade I (WHO CNS 2021) (2.9 %) suprasellar mature teratoma, one (2.9 %) chondrosarcoma, and one (2.9 %) epidermioid cyst. Histological features are reported in Table 1.

Among PitNETs, a mixed somatotroph-lactotrophinoma had been

Table 1
Histological features of the series.

Tumor		N.	Percentage
Pituitary Neuroendocrine Tumor (PitNET)	Gonadotroponoma	13	37.1 %
	Plurihormonal Pit-1	3	8.6 %
	Silent Corticotropinomas	3	8.6 %
	Mixed Somatotroph-Lactotrophinoma	1	2.9 %
Meningioma	Meningothelial	7	20.0 %
	With Oncocitic Features	2	5.7 %
Craniopharyngiomas	Adamantinomatous	1	2.9 %
	Papillary	1	2.9 %
Pilocytic Astrocytoma		1	2.9 %
Mature Teratoma		1	2.9 %
Chondrosarcoma		1	2.9 %
Epidermioid cyst		1	2.9 %

treated for three months with long-acting somatostatine and cabergoline before surgery, while 3 (8.6 %) had already undergone endoscopic endonasal surgery.

Basal pituitary function was normal in 30/35 (85.7 %) patients; 3 presented with anterior hypopituitarism and 1 with panhypopituitarism and diabetes insipidus.

At baseline, 22 out of 35 (62.9 %) patients presented with visual symptoms consisting of temporal hemianopsia in 13 (37.1 %), left hemianopsia in 5 (14.3 %), and right hemianopsia in 4 (11.4 %).

3.2. Clinical follow-up

Radical tumor removal was achieved in 27/35 (77.1 %) cases. Complications consisted in one case of cerebrospinal fluid leak with meningitis and one abscess inside the surgical field, both requiring endoscopic endonasal re-intervention; one chronic subdural hematoma; and two transient diabetes insipidus.

GH/prolactin hypersecretion was normalized after surgery therefore no subsequent treatment was required. At 12-month follow-up, pituitary function was preserved in 27 cases (77.1 %); the two patients with pre-operative anterior hypopituitarism were stable; 3 patients developed de novo partial anterior hypopituitarism (8.6 %), and two patients anterior panhypopituitarism and diabetes insipidus.

Resolution of visual symptoms was complete in 8 (36.4 %) and partial in 14 (63.6 %) out of 22 patients. No deterioration of visual functioning was observed.

3.3. Neuroradiological anatomical comparison

The quality of all 3D MPRAGE T1-weighted and CISS images was deemed good (i.e., absence of movement artifacts). In five patients it was not possible to acquire CISS. Upon visual inspection of the 3D MPRAGE T1-weighted images, the AOP was considered “perfectly visible” in the initial validation subsample of healthy controls. It was “perfectly visible” in 24/35 (68.6 %) patients, “partially visible” in 11/35 (31.4 %), and “not visible” in none. Specifically, the optic nerves (either left or right) were not visible in 8/35 (22.9 %) patients, the optic chiasm in 4/35 (11.4 %), and the optic tracts (either left or right) in 3/35 (8.6 %).

Regarding CISS images, the AOP was considered “perfectly visible” in the initial validation subsample of healthy controls. Among the patients, it was “perfectly visible” in 17/35 patients (48.6 %), “partially visible” in 13/35 (37.1 %) patients and “not visible” in none, specifically, the optic nerves (either left or right) were not visible in 9/35 (25.7 %), patients, the optic chiasm in 5/35 (14.3 %), and the optic tracts (either left or right) in 3/35 (8.6 %).

Overall, there were 11/35 (31.4 %) cases where the AOP was not fully visible either on the T1-weighted or the CISS image.

In 28/35 (80.0 %) cases the tumor had displaced the optic chiasm.

In all instances where the AOP was detectable on MPRAGE images, the automated tractography reconstruction accurately overlaid the T1-weighted images. Visual examples are shown in Fig. 3. Additionally, the brains of the same subjects are represented in Supplementary Fig. 3, showing the T1-weighted image side-by-side with the AOP reconstruction, to allow readers to better appreciate the identification of the automated pipeline.

Cranio-caudal chiasmal displacement (i.e., B-P height > 1 mm) was observed in 28/35 (80.0 %) patients. The mean B-P height measured on the 3D T1 MPRAGE images of those patients was 9 ± 5 mm (range: 2–18 mm).

3.4. Neurosurgical confirmation

At surgical inspection, a correct correspondence of all AOP segments was identified in 11/13 (84.7 %) patients. It was impossible to confirm the corrected reconstruction of the right and left optic tracts in two patients since they were not visible in the surgical field. Overall, 61/65 (93.8 %) portions of the AOP (i.e., left/right optic nerve, optic chiasm, left/right optic tract) across 13 patients were surgically confirmed.

3.5. Along-tract analysis

The along-tract alterations of microstructural parameters and their significance are summarized in Fig. 4.

Patients had significantly lower mean FA and FD values in the bilateral optic tract and optic nerve as compared to controls, while no significant differences were found in the other parts of the chiasm. MD values decreased bilaterally at the level of the chiasm and optic nerve, with focal increases in the extremal portion of the optic nerve and the central portion of the optic tract.

No significant differences in DTI metrics were detected after correction for multiple comparisons between patients with post-surgical resolution of the visual symptoms as compared to those who did not recover (data not shown). Results of the comparison between healthy controls and the visual field deficit subgroups are reported in Part 4 of the Supplementary Material.

The chiasmal displacement measure negatively correlated with the average MD value within the optic chiasm ($R = -0.49$; $p = 0.01$) in the 28 patients exhibiting a predominantly cranio-caudal displacement of the optic chiasm.

4. Discussion

To our knowledge, this study presents the largest series of subjects, both healthy and with SPTs, in which the AOP was completely reconstructed using a fully automated approach. The most used strategy for AOP automatic tractography reconstruction involves selecting ROIs based on anatomical atlases or a reference subpopulation, which are then aligned to the diffusion-weighted space of the individual subjects (Carrozzi et al., 2023). While this method yields optimal results when the anatomy is within normal limits, it has limitations in cases where the anatomy is altered, particularly when the chiasm is displaced due to an expansive process, a scenario in which tractography can be clinically useful. To address this issue, we employed an innovative strategy that relies on signal analysis of T1-weighted images to generate automatic ROIs of the optic chiasm. This approach produced anatomically accurate reconstructions even in severe dislocations of this structure and showed excellent results across all situations, potentially reducing spurious pathways in the final tracts.

These post-processing techniques, which can be implemented by an MR specialist who has multishell acquisitions and advanced image processing software at their disposal, represent a decisive simplification of image processing compared to the conventionally employed manual approach and could favor a wider application of the technique in clinical practice, at least in hospital facilities where advanced imaging and minimally invasive surgery techniques are available. Indeed, manual ROI definition is known to be a time-consuming process that requires

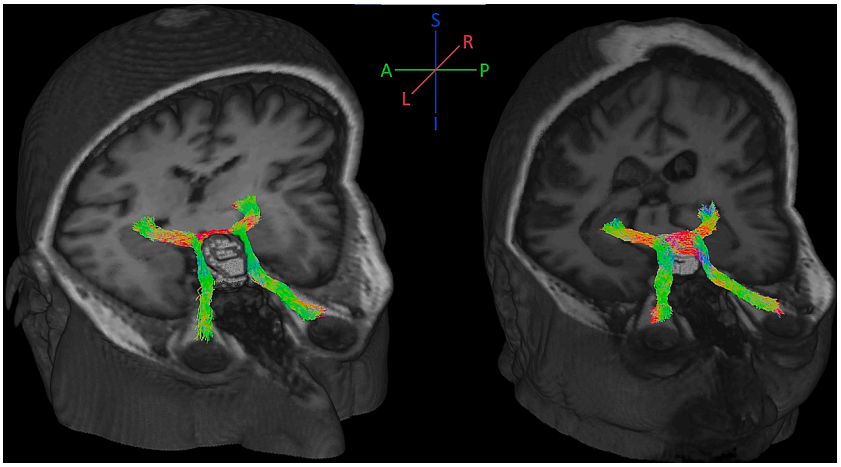

Fig. 3. Example of the reconstruction of the anterior optic pathway using the automated pipeline in two patients with severe displacement of the optic chiasm in the posterior (left) and superior (right) directions.

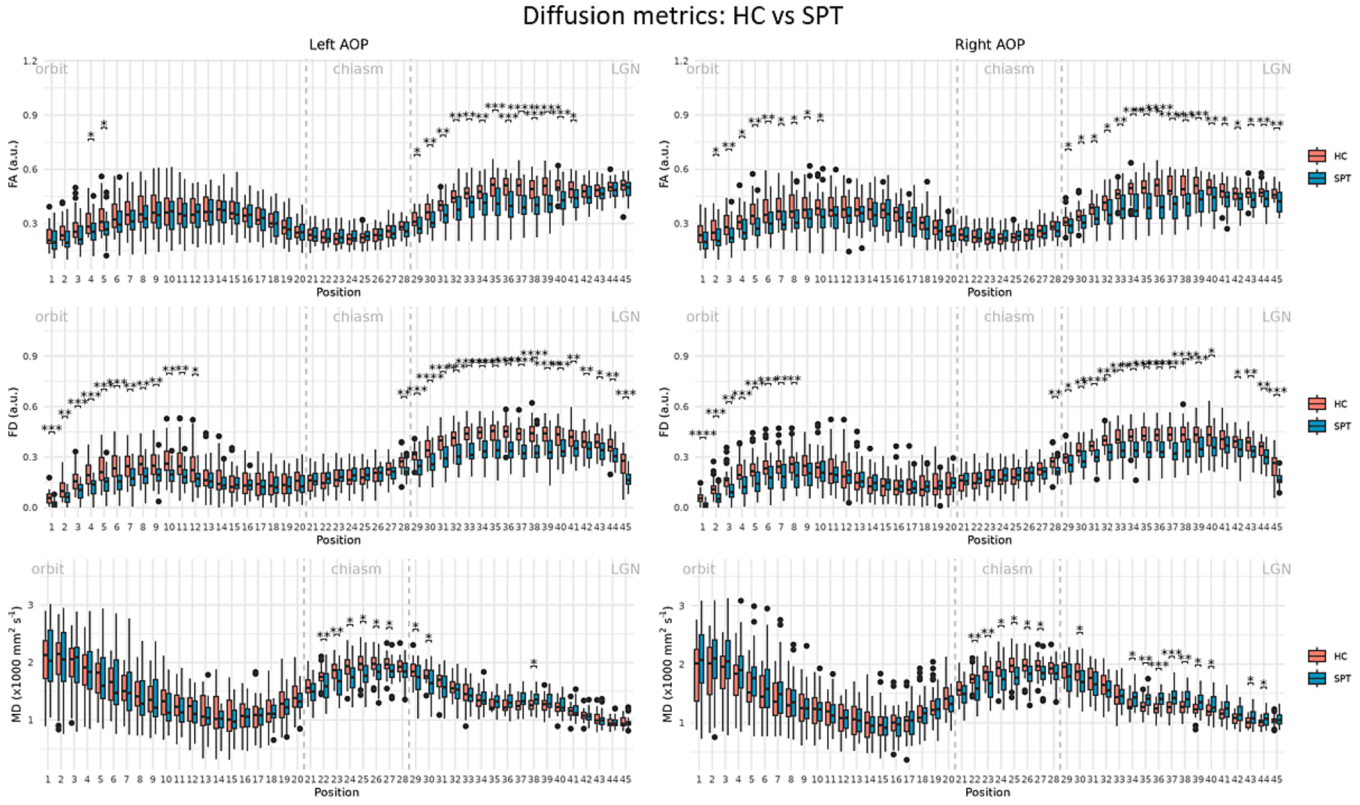

Fig. 4. Along-tract analysis of fractional anisotropy, mean diffusivity, and fixel density for left (left) and right (right) anterior optic pathway in patients (blue = SPT) and controls (red = HC). Position 1 = eye orbit, position 45 = lateral geniculate nucleus. * = adjusted $p < 0.05$; ** = adjusted $p < 0.01$; *** = adjusted $p < 0.001$; **** = adjusted $p < 0.0001$. Cond = condition, HC = healthy controls, SPT = Sellar/parasellar tumors, FA = fractional anisotropy, MD = mean diffusivity, FD = fixel density. (For interpretation of the references to colour in this figure legend, the reader is referred to the web version of this article.)

knowledge and experience (Jacquesson et al., 2018b), representing a limiting factor for the spread of tractography outside the clinical research environment.

The anatomical fidelity of our reconstruction method was confirmed through *in vivo* inspection during surgery in 13 out of 35 patients, showing a high level of agreement (85 %) in accurately depicting the 3D dislocation of the tract and reflecting true anatomy, marking an improvement over to conventional techniques based on 3D structural imaging, such as T1-weighted or CISS sequences, through which AOP was fully visible only in 68.6 % of the cases.

Based on these preliminary results, which also showed good repeatability as shown in Part 3 of the Supplementary Material, the anatomical fidelity of the 3D reconstruction of the AOP is reliable, and shows promise as a tool for guiding presurgical planning in patients with SPTs.

The potential of AOP tractography to assist the surgical removal of SPTs using neuro-navigational systems has attracted the interest of the neurosurgical community (Jacquesson et al., 2018a), but no standard procedure to perform this reconstruction has been proposed. In our experience, it provided a precise spatial reference that increased the

surgeon's confidence during delicate maneuvers near the optic apparatus, helping to avoid inadvertent contact with the optic chiasm. While this improved precision could not be measured, in our series no damage of the chiasma was reported. Hodaie et al. (Hodaie et al., 2010) were pioneers in attempting the *in vivo* reconstruction of CNs in 4 neurosurgical patients, and achieved reconstructions that closely matched the established anatomy for CNs II, III, V, and the VII-VIII bundle. This demonstrated the potential utility of the technique for diagnostic procedures and surgical planning in neurosurgery. Lober et al. (Lober et al., 2012) attempted the retrospective reconstruction of the anterior optic pathway in 10 pediatric patients with optic glioma using a standard MRI acquisition (25 isotropic direction with b-value = 1000 s/mm^2 and a 3 mm thickness) and a deterministic software (InVivo Dynasuite). Interestingly, the authors found that two patients had an unexpected displacement of the non-tumor fiber bundle by the chiasm, and this might have been helpful for the pre-operative planning if they had been identified before surgery. Yoshino et al. (Yoshino et al., 2016) successfully reported the surgical confirmation of CN reconstruction by tractography in three patients. The image findings were considered critical in choosing the surgical approach in a 35-year-old woman with an optic-hypothalamic glioma in which a presurgical predominant inferior displacement of the optic chiasm was found and a supraorbital approach was preferred over an endonasal approach. The adoption of AOP tractography with neuronavigation allows for the intraoperative anticipation of the optic nerves and chiasm's location, even when obscured by a tumor or other structures. This information helps avoid potentially dangerous maneuvers, such as drilling or sharp incisions near these delicate structures, thereby reducing the risk of unintended manipulation.

Based on all the previously reported experiences (Carrozzi et al., 2023), AOP tractography also seems useful pre-operatively to guide the neurosurgeon in planning the most appropriate approach for each case. Briefly, the endoscopic endonasal approach is preferable when the chiasm is displaced postero-superiorly. Conversely, if the tumor pushes these structures antero-inferiorly, toward the tuberculum sellae along the ventral surgical trajectory, an alternative approach, such as a transcranial route, should be considered.

In our experience, tractography successfully visualized the optic chiasm in all cases, compared to 85.2 % visualization rate with 3D MPRAGE T1-weighted and 77.3 % with CISS. Preoperative tractography provided the surgeon with crucial information regarding the presence of a favorable surgical corridor, allowing for the avoidance of contact with the optic chiasm. Indeed, the possibility of providing reliable information about the relationship between the AOP and the neoplasm could have a significant impact on the choice of the surgical approach. As demonstrated by several studies, the optic nerve plane represents the lateral limit of the endoscopic endonasal approach, and tumors with a significant transgression of this limit require an open transcranial approach. Since conventional imaging cannot provide this feature in all cases, especially for the most complex tumors, the adoption of AOP tractography can represent a valuable tool for selecting patients who are candidates for the endoscopic endonasal approach. Additionally, the possibility of intra-operatively assisting the surgical resection through the adoption of AOP reconstruction in neuronavigation, coupled with the refinement of pre-operative information for choosing the approach, makes tractography a promising technological contribution to decreasing surgical morbidity and improving ophthalmological outcomes in patients with sellar/parasellar tumors.

After a successful tractography reconstruction of the AOP has been achieved, it is possible to extract diffusion metrics within the tract. Based on the hypothesis that these may be correlated to clinical parameters to yield a biological interpretation, we explored the clinical correlations of the metrics inside the tracts and discovered significant differences between patients and healthy controls. Specifically, there was a notable reduction in MD values within the optic chiasm and a reduction in FA and FD in the optic tracts and optic nerves of patients. These findings are consistent with existing literature, which also reports a reduction in FA values in similar patient populations (Liang et al., 2021; Wu et al., 2019; Anik et al., 2011; Paul et al., 2014; Raz et al., 2015); while there are no previous reports on the FD in the AOP, it demonstrated higher sensitivity compared to FA in detecting alterations in this structure. The FD provides a relative measure of the intra-axonal volume occupied by fibers aligned with a specific direction; similarly to FA, in this context, the reduction of FD in patients may be interpreted as a loss of density and coherence of the fiber population in the optic nerves and tracts.

The finding of the decrease in MD at the level of the displaced optic chiasm is interesting and its interpretation challenging.

A prior histological study on post-mortem models of optic nerve compression (Clifford-Jones et al., 1985)—where animals were implanted with an inflatable balloon in the orbit—demonstrated an increase in remyelinating fibers leading to an increased cellularity and membrane density in the compressed areas. In particular, the authors found that within the first week, the predominant pathological change was demyelination. Moreover, both partially and completely demyelinated fibers were seen at all stages of the experiments, but, by the fifth week, some axons had been remyelinated by oligodendrocytes despite the continued presence of the balloon.

This led to increased cellularity and membrane density within the compressed nerve, changes that are commonly associated with reduced ADC values (Le Bihan et al., 2001).

Similarly, a previous study in patients with vestibular schwannomas (Halawani, 2020) reported a reduction in MD in the compressed nerves, possibly due to increased number of glial layers within a confined space. In line with this, it has been demonstrated in cellular models that the length of the biological membrane is one of the independent predictors of ADC values (Eida et al., 2016).

The reduction of FA values in the optic tracts and optic nerves in patients with SPTs compressing the AOP confirms previously published data (Liang et al., 2021; Wu et al., 2019; Anik et al., 2011; Paul et al., 2014; Raz et al., 2015) and was not associated with the probability of visual recovery. This supports the previously reported concept that, despite abnormal FA values within the tracts, patients can still experience complete resolution of visual symptoms. It is worth noting that patients with lesions displacing the chiasm do not show a reduction in visual acuity, but rather in the width of the visual field. Wu et al. (Wu et al., 2019), using a DTI analysis of a single-shell acquisition and b = 1000 s/mm^2, found asymmetry in the FA values of the optic nerves of patients with mono-orbital space-occupying lesions who presented a reduction in visual acuity, but not a reduction in the width of the visual field.

Although we observed that AOP tractography reconstruction is feasible for visualizing the anterior optic tract and chiasmal displacement, we did not find a strong correlation between preoperative DTI parameters and postoperative visual function recovery. This may be due to the fact that reduced FA and increased diffusivity do not necessarily indicate irreversible damage. Moreover, visual recovery may occur over weeks to months, involving mechanisms such as neuroplasticity and remyelination, which are not captured by preoperative imaging. Interestingly, we observed that the distribution of along-tract diffusion metrics corresponded to the clinical symptoms of the patients. In particular, in the subgroup of patients presenting with bitemporal visual field deficits (n = 12), consistent with chiasmal compression, we identified a marked reduction in MD whereas in patients with unilateral hemianopia more pronounced reductions in FA in the optic tract were found. Although these observations are limited by the small sample size within each subgroup (n = 5 for left hemianopia, n = 4 for right hemianopia), they suggest that the along tract tractography metrics may reflect the severity and anatomical pattern of visual impairment at presentation, supporting the evaluation of clinical assessment—particularly in patients for whom reliable visual field testing is not feasible preoperatively.

In our study, we have broadened the clinical application of multishell DWI acquisition for the reconstruction of the cranial nerves, originally performed on a small cohort of five patients with Vestibular Schwannoma to reconstruct the facial nerve (Castellaro et al., 2020). We have developed a framework that facilitates the semi-automatic generation of 3D reconstructions of the anterior optic pathway to support the dissemination and integration of this DWI sequence into the workflow of presurgical planning for endoscopic endonasal procedures. Additionally, we found microstructural alterations of the AOP consistent with local compression or gliosis of the optic chiasm due to the tumor.

The limited sample size of 13 patients for the *in vivo* neurosurgical validation represents the main study limitation. However, in this subset —referred to as the neurosurgical validation subset— all segments visible in the surgical view corresponded with those anticipated by the tractography reconstruction. Although preliminary, these findings support the reliability of the method; conversely, pairs of optic tracts not visible during surgery could not be validated and their absence did not necessarily indicate an erroneous reconstruction. This was deemed sufficient to confirm the correspondence with the real anatomy. However, it must be noted that the largest portion of the SPT patient group, i.e. 22/35 subjects, could not receive direct intraoperative validation through surgical inspection. Another limitation is that the AOP is a small structure, and runs close to tissue interfaces, including CSF/subarachnoid cistern spaces, meaning that tract-derived diffusion metrics could be influenced by tissue partial volume effects. A last limitation to the broader applicability of our study is the requirement for high-quality data acquisition, such as isotropic multishell DWI, along with dedicated data analysis. However, we demonstrate that the technique is technically feasible and reproducible. The use of an automated evaluation pipeline, including the automatic selection of the optic chiasm ROI, may further support the implementation of this protocol across centers without specific expertise in tractography of the anterior visual pathway. This could facilitate the integration of advanced neuroimaging techniques into clinical practice through multicentric studies.

5. Conclusions

An innovative and completely automated technique for tractography of the AOP was created and successfully tested in surgical practice in patients harboring SPTs. The high correspondence between the reconstructions and the surgical anatomy supports the validity of the method. This technological tool can have a positive impact both in the refinement of patient selection for an endoscopic endonasal vs. an open transcranial approach and in guiding the surgeon during the tumor resection, thus reducing the involuntary manipulation of the optic structures and thus potentially improving clinical outcomes. Moreover, novel insights on the effect of SPTs on microstructural diffusion parameters in the optic chiasm were revealed and correlated with chiasmal displacement, indicating hypercellularity or chiasmal compression as the plausible origins of such alterations.

CRediT authorship contribution statement

Laura Ludovica Gramegna: Writing – review & editing, Writing – original draft, Methodology, Formal analysis, Data curation, Conceptualization. **Matteo Zoli:** Writing – review & editing, Writing – original draft, Project administration, Methodology, Data curation, Conceptualization. **Giovanni Sighinolfi:** Writing – review & editing, Writing – original draft, Methodology, Formal analysis. **Alessandro Carrozzi:** Writing – review & editing, Writing – original draft, Formal analysis. **Gianfranco Vornetti:** Writing – review & editing, Formal analysis. **Elena Cantoni:** Writing – review & editing, Formal analysis. **Federica Guaraldi:** Writing – review & editing, Data curation. **Sofia Asioli:** Writing – review & editing, Data curation. **Caterina Tonon:** Writing – review & editing, Supervision, Resources, Project administration, Funding acquisition, Conceptualization. **David Neil Manners:** Writing – review & editing, Writing – original draft, Formal analysis. **Diego Mazzatenta:** Writing – review & editing, Supervision, Project administration, Data curation, Conceptualization. **Raffaele Lodi:** Writing – review & editing, Supervision, Project administration, Funding acquisition, Conceptualization.

Declaration of competing interest

The authors declare that they have no known competing financial interests or personal relationships that could have appeared to influence the work reported in this paper.

Acknowledgements

This work has been supported by Fondazione Cassa di Risparmio di Bologna (CARISBO, project No. 2020.0408), MNESYS (project No. PE0000006), and by the Italian Ministry of Health ("Ricerca Corrente").

Appendix A. Supplementary data

Supplementary data to this article can be found online at https://doi.org/10.1016/j.nicl.2025.103827.

Data availability

Numerical data of microstructural diffusion parameters and relevant clinical features are deposited on the open access platform Zenodo (https://zenodo.org/) and made available upon request to the corresponding author (https://doi.org/10.5281/zenodo.13354115).

References

Anik, I., Anik, Y., Koc, K., Ceylan, S., Genc, H., Altintas, O., Ozdamar, D., Ceylan, D.B., 2011. Evaluation of early visual recovery in pituitary macroadenomas after endoscopic endonasal transphenoidal surgery: quantitative assessment with diffusion tensor imaging (DTI). Acta Neurochir. 153 (4), 831–842. https://doi.org/10.1007/s00701-011-0942-4.

Barazi, S.A., Pasquini, E., D'Urso, P.I., Zoli, M., Mazzatenta, D., Sciarretta, V., Frank, G., 2012. Extended endoscopic transplanum–transtuberculum approach for pituitary adenomas. Br. J. Neurosurg. 27 (3), 374–382. https://doi.org/10.3109/02688697.2012.741739.

Basser, P.J., Pajevic, S., Pierpaoli, C., Duda, J., Aldroubi, A., 2000. In vivo fiber tractography using DT-MRI data. Magn. Reson. Med. 44 (4), 625–632. https://doi.org/10.1002/1522-2594(200010)44:4<625::aid-mrm17>3.0.co;2-o.

Beare, R., Alexander, B., Warren, A., Kean, M., Seal, M., Wray, A., Maixner, W., Yang, J.-M., 2023. Karawun: a software package for assisting evaluation of advances in multimodal imaging for neurosurgical planning and intraoperative neuronavigation. Int. J. Comput. Assist. Radiol. Surg. 18 (1), 171–179. https://doi.org/10.1007/s11548-022-02736-7.

Benjamini, Y., Hochberg, Y., 1995. Controlling the false discovery rate: a practical and powerful approach to multiple testing. J. R. Stat. Soc. Ser. B Stat Methodol. 57 (1), 289–300. https://doi.org/10.1111/j.2517-6161.1995.tb02031.x.

Carretta, A., Zoli, M., Guaraldi, F., Sollini, G., Rustici, A., Asioli, S., Faustini-Fustini, M., Pasquini, E., Mazzatenta, D., 2023. Endoscopic endonasal transplanum-transtuberculum approach for pituitary adenomas/PitNET: 25 years of experience. Brain Sci. 13 (7), 1121. https://doi.org/10.3390/brainsci13071121.

Carrozzi, A., Gramegna, L.L., Sighinolfi, G., Zoli, M., Mazzatenta, D., Testa, C., Lodi, R., Tonon, C., Manners, D.N., 2023. Methods of diffusion MRI tractography for localization of the anterior optic pathway: a systematic review of validated methods. NeuroImage. Clinical 39, 103494. https://doi.org/10.1016/j.nicl.2023.103494.

Castellaro, M., Moretto, M., Baro, V., Brigadoi, S., Zanoletti, E., Anglani, M., Denaro, L., et al., 2020. Multishell diffusion MRI-based tractography of the facial nerve in vestibular schwannoma. AJNR Am. J. Neuroradiol. 41 (8), 1480–1486. https://doi.org/10.3174/ajnr.A6706.

Clifford-Jones, R.E., McDonald, W.I., Landon, D.N., 1985. Chronic optic nerve compression an experimental study. Brain 108 (1), 241–262. https://doi.org/10.1093/brain/108.1.241.

Cox, R.W., 1996. AFNI: software for analysis and visualization of functional magnetic resonance neuroimages. Comput. Biomed. Res. 29 (3), 162–173. https://doi.org/10.1006/cbmr.1996.0014.

Dhollander, Thijs, Remika Mito, David Raffelt, and Alan Connelly. 2019. 'Improved White Matter Response Function Estimation for 3-Tissue Constrained Spherical Deconvolution'. In . https://archive.ismrm.org/2019/0555.html.

Eida, S., Van Cauteren, M., Hotokezaka, Y., Katayama, I., Sasaki, M., Obara, M., Okuaki, T., Sumi, M., Nakamura, T., 2016. Length of intact plasma membrane

determines the diffusion properties of cellular water. Sci. Rep. 6 (January), 19051. https://doi.org/10.1038/srep19051.
Frisén, L., Jensen, C., 2008. How robust is the optic chiasm? Perimetric and neuro-imaging correlations. Acta Neurol. Scand. 117 (3), 198–204. https://doi.org/10.1111/j.1600-0404.2007.00927.x.
Gaillard, Frank. 2025. 'WHO Classification of Endocrine and Neuroendocrine Tumours'. In *Radiopaedia.Org*. Radiopaedia.org. https://doi.org/10.53347/rid-212576.
Halawani, Aisha. 2020. 'Correlation between Cranial Nerve Microstructural Characteristics and Vestibular Schwannoma Tumor Volume', May. https://doi.org/10.26226/morressier.5e8335ba7cb08a046ef7c71c.
He, J., Zhang, F., Xie, G., Yao, S., Feng, Y., Bastos, D.C.A., Rathi, Y., et al., 2021. Comparison of multiple tractography methods for reconstruction of the retinogeniculate visual pathway using diffusion MRI. Hum. Brain Mapp. 42 (12), 3887–3904. https://doi.org/10.1002/hbm.25472.
Hodaie, M., Quan, J., Chen, D.Q., 2010. In vivo visualization of cranial nerve pathways in humans using diffusion-based tractography. Neurosurgery 66 (4), 788–796. https://doi.org/10.1227/01.neu.0000367613.09324.da.
Jacquesson, T., Cotton, F., Attyé, A., Zaouche, S., Tringali, S., Bosc, J., Robinson, P., Jouanneau, E., Frindel, C., 2018a. Probabilistic tractography to predict the position of cranial nerves displaced by skull base tumors: value for surgical strategy through a case series of 62 patients. Neurosurgery 85 (1), E125–E136. https://doi.org/10.1093/neuros/nyy538.
Jacquesson, T., Frindel, C., Kocevar, G., Berhouma, M., Jouanneau, E., Attyé, A., Cotton, F., 2018b. Overcoming challenges of cranial nerve tractography: a targeted review. Neurosurgery 84 (2), 313–325. https://doi.org/10.1093/neuros/nyy229.
Jenkinson, M., Beckmann, C.F., Behrens, T.E.J., Woolrich, M.W., Smith, S.M., 2012. FSL. Neuroimage 62, 782–790.
Jeurissen, B., Descoteaux, M., Mori, S., Leemans, A., 2017. Diffusion MRI fiber tractography of the brain. NMR Biomed. 32 (4). https://doi.org/10.1002/nbm.3785.
Jeurissen, B., Tournier, J.-D., Dhollander, T., Connelly, A., Sijbers, J., 2014. Multi-tissue constrained spherical deconvolution for improved analysis of multi-shell diffusion MRI data. Neuroimage 103 (December), 411–426. https://doi.org/10.1016/j.neuroimage.2014.07.061.
Jones, Derek K. 2010. 'Optimal Approaches to Diffusion MRI Acquisition'. *Diffusion MRI*, November, 250–71. https://doi.org/10.1093/med/9780195369779.003.0015.
Bihan, L., Denis, J.-F., Poupon, C., Clark, C.A., Pappata, S., Molko, N., Chabriat, H., et al., 2001. Diffusion tensor imaging: concepts and applications. J. Magn. Reson. Imaging 13 (4), 534–546. https://doi.org/10.1002/jmri.1076.
Liang, L., Lin, H., Lin, F., Yang, J., Zhang, H., Zeng, L., Yaqiong, Hu., et al., 2021. Quantitative visual pathway abnormalities predict visual field defects in patients with pituitary adenomas: a diffusion spectrum imaging study. Eur. Radiol. 31 (11), 8187–8196. https://doi.org/10.1007/s00330-021-07878-x.
Lober, R.M., Guzman, R., Cheshier, S.H., Fredrick, D.R., Edwards, M.S.B., Yeom, K.W., 2012. Application of diffusion tensor tractography in pediatric optic pathway glioma. J. Neurosurg. Pediatr. 10 (4), 273–280. https://doi.org/10.3171/2012.7.peds1270.
Manners, D.N., Gramegna, L.L., La Morgia, C., Sighinolfi, G., Fiscone, C., Carbonelli, M., Romagnoli, M., Carelli, V., Tonon, C., Lodi, R., 2022. Multishell diffusion MR tractography yields morphological and microstructural information of the anterior optic pathway: a proof-of-concept study in patients with Leber's hereditary optic neuropathy. Int. J. Environ. Res. Public Health 19 (11), 6914. https://doi.org/10.3390/ijerph19116914.
Mikami, T., Minamida, Y., Yamaki, T., Koyanagi, I., Nonaka, T., Houkin, K., 2005. Cranial nerve assessment in posterior fossa tumors with fast imaging employing steady-state acquisition (FIESTA). Neurosurg. Rev. 28 (4), 261–266. https://doi.org/10.1007/s10143-005-0394-5.
Paul, D.A., Gaffin-Cahn, E., Hintz, E.B., Adeclat, G.J., Zhu, T., Williams, Z.R., Edward Vates, G., Mahon, B.Z., 2014. White matter changes linked to visual recovery after nerve decompression. Sci. Transl. Med. 6 (266), 266ra173-266ra173. https://doi.org/10.1126/scitranslmed.3010798.
Puzniak, R.J., Ahmadi, K., Kaufmann, J., Gouws, A., Morland, A.B., Pestilli, F., Hoffmann, M.B., 2019. Quantifying nerve decussation abnormalities in the optic chiasm. NeuroImage. Clinical 24, 102055. https://doi.org/10.1016/j.nicl.2019.102055.
Raffelt, D.A., Tournier, J.-D., Smith, R.E., Vaughan, D.N., Jackson, G., Ridgway, G.R., Connelly, A., 2017. Investigating white matter fibre density and morphology using fixel-based analysis. Neuroimage 144 (Pt A), 58–73. https://doi.org/10.1016/j.neuroimage.2016.09.029.
Raffelt, D., Tournier, J.-D., Rose, S., Ridgway, G.R., Henderson, R., Crozier, S., Salvado, O., Connelly, A., 2012. Apparent fibre density: a novel measure for the analysis of diffusion-weighted magnetic resonance images. Neuroimage 59 (4), 3976–3994. https://doi.org/10.1016/j.neuroimage.2011.10.045.
Raz, N., Bick, A.S., Klistorner, A., Spektor, S., Reich, D.S., Ben-Hur, T., Levin, N., 2015. Physiological correlates and predictors of functional recovery after chiasmal decompression. J. Neuro-Ophthalmol. 35 (4), 348–352. https://doi.org/10.1097/WNO.0000000000000266.
Tournier, J.-D., Fernando, C., Alan, C., 2012. MRtrix: diffusion tractography in crossing fiber regions. Int. J. Imaging Syst. Technol. 22 (1), 53–66. https://doi.org/10.1002/ima.22005.
Veraart, J., Novikov, D.S., Christiaens, D., Ades-Aron, B., Sijbers, J., Fieremans, E., 2016. Denoising of diffusion MRI using random matrix theory. Neuroimage 142 (November), 394–406. https://doi.org/10.1016/j.neuroimage.2016.08.016.
Wu, C.-N., Duan, S.-F., Xue-Tao, M., Wang, Y., Lan, P.-Y., Wang, X.-L., Li, K.-C., 2019. Assessment of optic nerve and optic tract alterations in patients with orbital space-occupying lesions using probabilistic diffusion tractography. Int. J. Ophthalmol. 12 (8), 1304–1310. https://doi.org/10.18240/ijo.2019.08.11.
Yoshino, M., Abhinav, K., Yeh, F.-C., Panesar, S., Fernandes, D., Pathak, S., Gardner, P.A., Fernandez-Miranda, J.C., 2016. Visualization of cranial nerves using high-definition fiber tractography. Neurosurgery 79 (1), 146–165. https://doi.org/10.1227/neu.0000000000001241.
Zoli, M., Guaraldi, F., Zenesini, C., Acciarri, N., Sollini, G., Asioli, S., Faustini-Fustini, M., et al., 2022. Role of endoscopic endonasal approach for craniopharyngiomas extending into the third ventricle in adults. Brain Spine 2 (June), 100910. https://doi.org/10.1016/j.bas.2022.100910.